PROCEEDINGS OF SCIENCE

Multi-wavelength inspection of the pre-starforming Dark Globule, DC 314.8-5.1: in search of cosmic-ray ionization

E. Kosmaczewski,[a,*] **C.C. Cheung,**[b] **Ł. Stawarz,**[c] **A. Bamba,**[d] **A. Karska,**[e,f] **W. R. M. Rocha**[g] **and S. S. Shenoy**[h]

[a] *National Research Council Research Associate, National Academy of Sciences, Washington DC 20001, USA; Resident at Naval Research Laboratory, Washington, DC USA*

[b] *Naval Research Laboratory, Washington, DC USA*

[c] *Astronomical Observatory of the Jagiellonian University, ul. Orla 171, 30-244 Kraków, Poland*

[d] *Department of Physics, Graduate School of Science, The University of Tokyo, 7-3-1 Hongo, Bunkyo-ku, Tokyo 113-0033, Japan*

[e] *Max-Planck-Institut für Radioastronomie, Auf dem Hügel 69, 53121, Bonn, Germany*

[f] *Institute of Astronomy, Faculty of Physics, Astronomy and Informatics, Nicolaus Copernicus University, ul. Grudziadzka 5, 87-100 Toruń, Poland*

[g] *Laboratory for Astrophysics, Leiden Observatory, Leiden University, P.O. Box 9513, NL 2300 RA Leiden, The Netherlands*

[h] *USRA-SOFIA Science Center, NASA Ames Research Center, Moffett Field, CA 94035, USA*

E-mail: emily.kosmaczewski.ctr@nrl.navy.mil

We present an analysis of the multi-wavelength observations of the dark globule, DC 314.8-5.1, using the optical survey Gaia, the near-infrared survey 2MASS, mid-infrared survey WISE along with dedicated imaging with the Spitzer Space Telescope, and finally X-ray data obtained with the Swift-XRT telescope. This cloud has a coincidental association with a B-type field star, which illuminates a reflection nebula within the cloud, resulting in infrared emission from the dust grains. The analysis of the infrared spectroscopy showed divergent physical conditions in the quiescent cloud DC 314.8-5.1 compared to molecular clouds with active star formation, which may indicate that cosmic rays were involved in the ionization of the system. Furthermore, our detailed analysis of the gathered multi-wavelength data confirms a very young, "pre-stellar core" evolutionary stage of the cloud, supporting the claim that the high ionization level may be the result of cosmic-ray interactions. All in all, our analysis indicates that DC 314.8-5.1 constitutes a compact reservoir of cold dust and gas, providing a truly unique insight into a primordial form of the interstellar medium.

38th International Cosmic Ray Conference (ICRC2023)
26 July - 3 August, 2023
Nagoya, Japan

*Speaker

PoS(ICRC2023)358

1. Introduction

The evolution of molecular clouds is strongly dependent on the development of star formation within such systems [for a review, see e.g.; 11]. The interactions of young stellar objects (YSOs), and the early stages of stellar formation, with their host clouds are substantial. Stars will form when the dense cores of these clouds collapse, with the infall of material resulting in the gravitational potential energy heating the material and increasing densities up to $\sim 10^8 - 10^9 \mathrm{cm}^{-3}$. The main effects of stellar formation are the processing of the dust within the cloud, the disruption of the cloud structure, and heating of the cloud material [13]. These processes continue as the system is altered and disrupted by the evolving young star. It is within this context that we study the molecular cloud, DC 314.8–5.1.

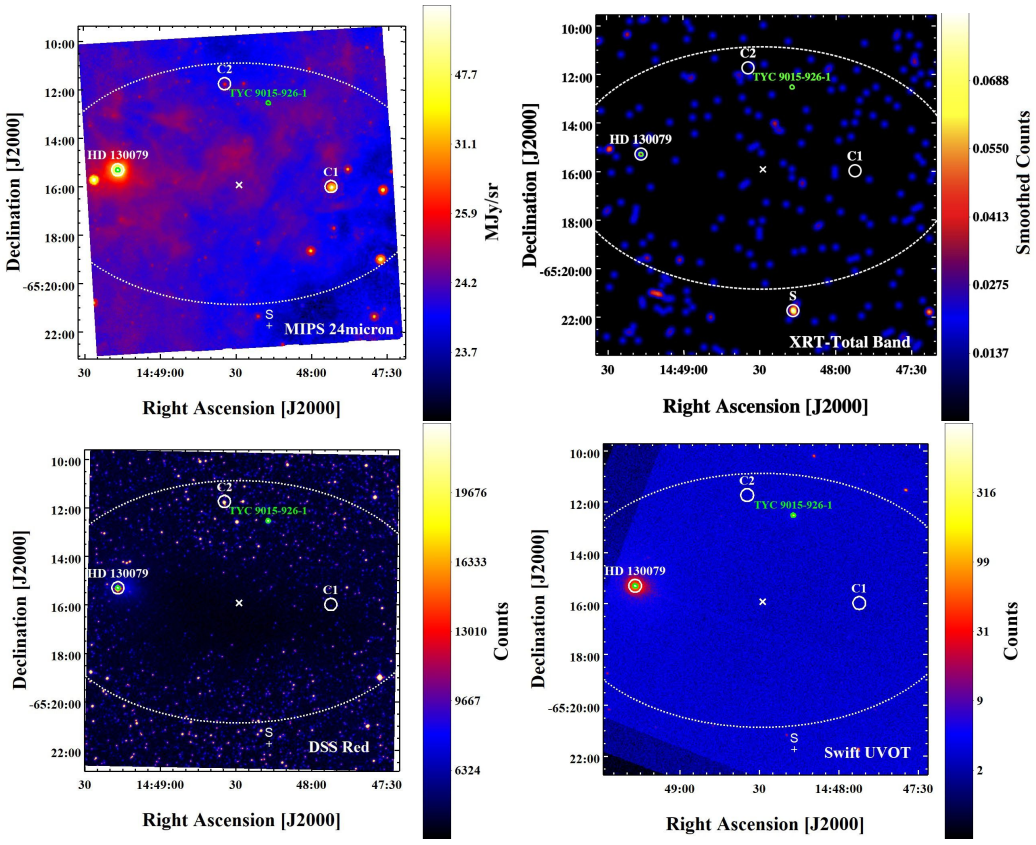

Figure 1: DC 314.8–5.1 region as seen at different wavelengths: (top left) Spitzer MIPS 24 μm log-scaled intensity mosaic map. (top right) Full-band 0.3–10 keV Swift XRT image of the DC 314.8–5.1 region, smoothed with a gaussian of radius 6 pixels. (bottom right) Swift UVOT M2–2250Å band log-scaled map. In each panel, the white dashed ellipse denotes the globule with the central position marked by a white"x". The green ellipses mark UVOT detected sources with HD 130079 marked on the left and TYC 9015-926-1 marked near the northern boundary of the globule. "C1" marks the YSO candidate identified by Whittet [28]. "C2" marks the YSO candidate identified in this work. The X-ray source detected with Swift-XRT is indicated by "S" with a cross. Figure from Kosmaczewski et al. [16]

The DC 314.8–5.1 dark globule is located approximately 5 deg below the Galactic plane in the southern constellation Circinus. The B9 V field star HD 130079, located near the cloud's eastern

boundary illuminates a reflection nebula [28]. The association of HD 130079 with DC 314.8–5.1 was established by van den Bergh & Herbst [27] who identified the presence of the reflection nebula utilizing the Palomar two-color survey, [20], of the southern sky. They further characterized the host cloud through absorption around the reflection nebulae determined from the density of field stars method. Later, Bourke et al. [4] used NH_3 observations to determine the physical characteristics (density, temperature, mass) of isolated dark clouds, including DC 314.8–5.1. The parallax value for HD 130079 in Gaia Early Data Release 3 [EDR3; 9], is 2.2981 ± 0.0194 mas. Bailer-Jones et al. [2] used the Gaia data and additional analyses to estimate the distance to the star as $431.7^{+3.2}_{-4.3}$ pc. Accordingly, the $\sim 7' \times 5'$ angular dimensions of the dark cloud [28], at 431.7 pc becomes a projected linear size of 0.9 pc × 0.6 pc. The extinction characteristics through the cloud imply a mean atomic hydrogen core number density $\sim 10^4\,\mathrm{cm}^{-3}$ and total cloud mass $\sim 160 M_\odot$ [see 28], at a distance of 431.7 pc.

We present here a highlight of the main findings of the spectroscopic and multi-wavelength studies of DC 314.8–5.1 originally presented in Kosmaczewski et al. [15] and Kosmaczewski et al. [16], respectively.

2. Data

We investigated the Spitzer Space Telescope Mid-Infrared spectroscopic data of DC 314.8–5.1 (Proposal ID 50039; P.I.: D. Whittet) the InfraRed Spectrograph [IRS; 12] Mapping mode, Infrared Array Camera [IRAC; 7] and the Multiband Imaging Photometer [MIPS; 21]. The data reduction procedure for spectroscopic data followed the CUBISM recipe outlined in the Spitzer Data Cookbook[1], Recipe 10, with parameters appropriate for our dataset outlined below [15].

The CUBISM standard bad pixel generation was applied with the following values: $\sigma_{trim} = 7$, minimum bad-fraction equal to 0.5 for global bad pixels and equal to 0.75 for record bad pixels. Due to the source being a low luminosity object, additional bad pixels were flagged visually before spectral extraction. 117 extraction regions were defined of dimensions 2×2 pixels around the field star, HD 130079, within the reflection nebula. Regions were selected such that the center of each new region was the edge of the previous region to account for subtle changes over distance. Spectral extraction was performed by selecting a region beginning on the star, of four pixels, and shifting the extraction region one pixels for each new extraction (in both vertical and horizontal directions)[26]. Each cube (i.e., each array of four neighbouring pixels), spans an angular width of $\sim 10''$.

Extracted spectra were fit utilizing the pypahdb[2] package [24]. The pypahdb package utilizes the NASA Ames PAH IR Spectroscopic Database [see 3, for an updated summary], to directly extract the ionization fraction and the size breakdown for the PAH molecules within the analyzed region by means of fitting the observed spectrum against the library of computed PAH spectra which contains data on thousands of PAH species. For our study, we fit with pypahdb for each of our sampled regions for the Spitzer SL1 mode (i.e. 7.5–15 μm). The resulting spectral fits have a high SNR > 5, with only five regions having 5 > SNR > 3, and only one region had an average residual equating a SN lower than 3 σ and as such was removed from any further analysis, see Figure 2.

[1] https://irsa.ipac.caltech.edu/data/SPITZER/docs/
[2] https://pahdb.github.io/pypahdb/

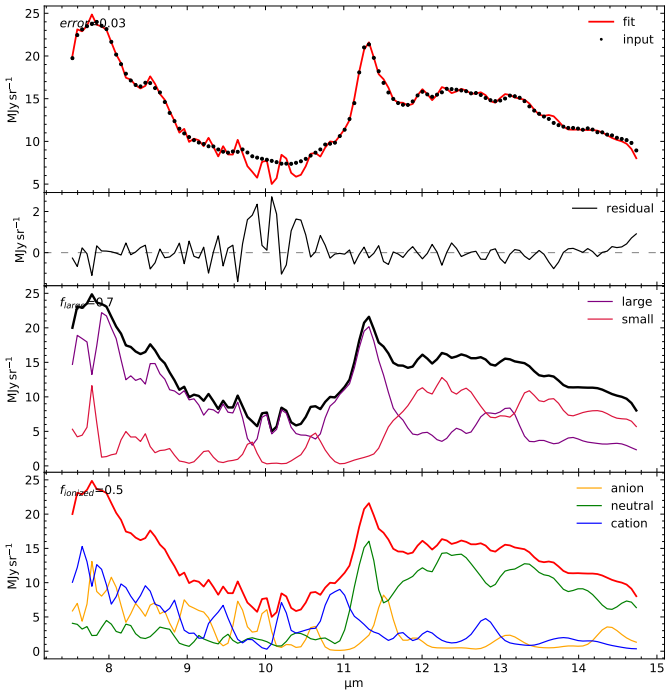

Figure 2: Pypahdb [24] fit of the SL1 mode from the nearest spectral region to HD 130079 at a projected distance of 0.03 pc. From top to bottom the individual panels represent: the fully fitted spectrum with data points marked as black dots with respective errors, note here that error bars are significantly small as to not be easily visible, residuals in the final fit, the breakdown of the PAH species sizes into large ($N_C > 40$) and small species, and the breakdown of the cation, neutral, and anion species. Figure from Kosmaczewski et al. [15]

The data reduction for the IRAC and MIPS images of DC 314.8–5.1 followed procedures outlines in the Spitzer Data Cookbook[3], and additional tools listed within, to produce mosaic maps in each band Kosmaczewski et al. [16]. Due to the presence of many bright sources within the field, we performed artifact correction utilizing the IRAC artifact mitigation tool. Reduction of the MIPS data similarly followed recipe 22 in the Spitzer Data Cookbook using MOPEX [18]. The resulting MIPS 24 μm map of the region, is shown in the top left panel of Figure 1.

3. Results & Discussions

The breakdown enabled by the pypahdb fitting, offers a direct view on the ionization fraction within DC 314.8–5.1. As shown in Figure 3, the ionized fraction returned by the fitting procedure, $n_{\mathrm{PAH+}}/(n_{\mathrm{PAH+}} + n_{\mathrm{PAH0}})$, is $\simeq 0.5$ within the regions of the cloud closest to the ionizing star, and decreasing somewhat down to $0.3 - 0.4$ at further distances, again with an increasing spread. These values therefore correspond to a ratio $n_{\mathrm{PAH+}}/n_{\mathrm{PAH0}} \simeq 1$ at the outskirts of the cloud, closer to the star, and down to $\sim 0.5 - 0.7$ at the furthest distances from the star probed in our analysis. Based on this, we therefore conclude that we do see an overall decrease in the ionization fraction with

[3] https://irsa.ipac.caltech.edu/data/SPITZER/docs/

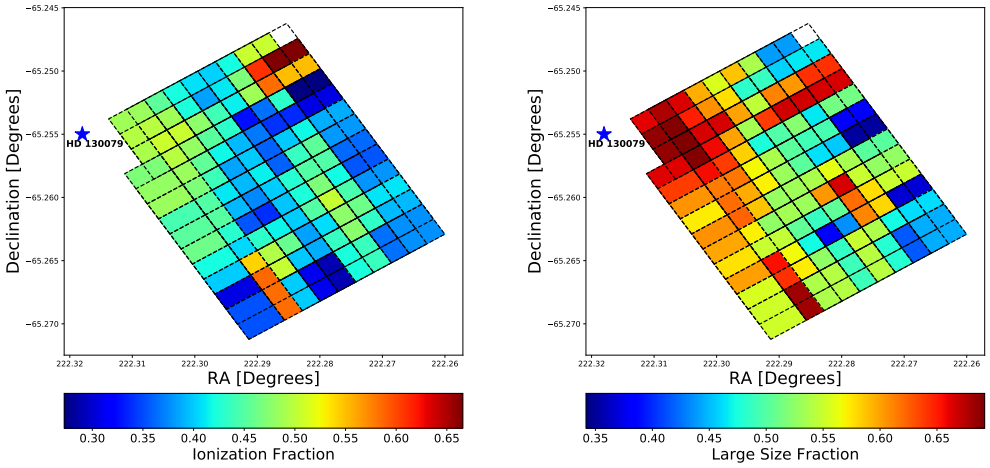

Figure 3: RA/DEC maps displaying the intensity of (left) the ionization fraction and (right) the large size fraction for the sampled regions. Figure from Kosmaczewski et al. [15]

distance, which is however much more modest than expected based solely on the decrease in the ionizing continuum from the star, hinting at the potential role of alternative ionization factors at play, such as ionization due to cosmic-rays [15].

Interestingly, the pypahdb fitting also provides insight into the large size fraction of the PAH molecules, where large molecules are defined as those with $N_C > 40$. The corresponding results are again shown in Figure 3, revealing that the PAH emission of the highly ionized regions at the cloud's boundaries, is dominated by large molecules (large size fraction > 0.6), which become less prevalent for the regions closer to the center of the cloud (large size fraction < 0.6), see Figure 3. We furthermore perform a basic correlation study between the two parameters, ionization and large size fractions, over all of the sampled regions with a SN ≥ 5. We utilize both a Pearson's product-moment correlation and Kendall's rank correlation. We find a statistically significant correlation with both methods, showing a statistic of 0.56 and 0.45 and p-value of 1.2×10^{-10} and 3.6×10^{-12} for Pearson's and Kendall's respectively [15].

To rule out the possibility of YSO interactions contributing to the higher ionization of the system we expanded on YSO identification methods for this system, utilizing data from dedicated observations with Spitzer and the Neil Gehrels Swift Observatory [5, Swift;], as well as from archival Wide-field Infrared Survey Explorer [30, WISE;], 2MASS [25], and Gaia [9] surveys [16].

The Spitzer IRAC mapping data, for the observed frame time of 12 seconds, effectively probes down to flux levels of 52 μJy at 8 μm, and 6.1 μJy at 3.6 μm with a spatial resolution of $\sim 2''$ [7]. At the distance of the cloud (432 pc), these limits correspond to monochromatic luminosities of $\simeq 4.4 \times 10^{29}$ erg s^{-1} and $\simeq 1.2 \times 10^{29}$ erg s^{-1}, respectively. The observed 3.6 μm range (3.1–3.9 μm), in particular, is rather close to the peak of the blackbody emission component in Class I–III sources, and as such the latter value should serve as a good proxy for the limiting luminosity of YSOs candidates, with the bolometric correction of the order of a few at most [see, e.g., 17]. In other words, in the Spitzer IRAC mapping data, we are sensitive to YSO Class I–III luminosities as low

as $\sim 10^{-4} L_\odot$, so that any young star with a core mass down to $0.01 M_\odot$ [see 6], should easily be detected.

We perform a search with a radius of 5′ around the central position of the cloud with the Spitzer Enhanced Imaging Products (SEIP) source list in order to identify potential YSOs. We restrict our sample by a signal-to-noise SNR > 5 in all four IRAC bands, excluding unresolved extended sources and excluding sources with only upper limits in any band. This returns a total of 1,319 sources. We apply the color criteria from [10, Appendix A.1],[29, Appendix A.2 (Eq. 17–20)], and [10, Appendix A.3] separately to the sample of 1,319 sources to identify Class I and II YSOs. None of the SEIP sources satisfied the criteria to be identified as a YSO, and as such these selections confirmed no candidate sources within DC 314.8–5.1 [16].

To identify potential Class III YSOs within DC 314.8–5.1 we utilize the AllWISE catalog, as discussed in Kang et al. [14]. We selected sources for the same region as the IRAC source selection, i.e. 5′, returning 618 sources. Following the cuts presented in [14], Section 3.1 and 3.2 therein, our sample contains one potential Class II object, and 34 potential Class III objects. The identified WISE source J144752.17-651601.1 fulfilling the color criteria for a Class II YSO, is the source identified as a possible YSO candidate by Whittet [28] based on 2MASS data. Class III sources, identified in this way, cannot be confidently distinguished from unrelated field stars and so with this in mind we further inspect these sources with the Gaia survey.

Gaia parallaxes provide precise measurements with a spatial resolution of 0.4″ and so are capable of separating individual objects even when clustered on the sky [9]. Using the distance values in Bailer-Jones et al. [2], we judge all candidates to be background stars reddened by dust along the line of sight. This is not surprising as many WISE identified Class III objects are consistent with reddened field stars. The remaining 33 potential YSO candidates are each coincident with a Gaia source and all have been excluded based on their parallax measurements exceeding the adopted distance to the cloud.

Furthermore we note that in the *Fermi* High-Latitude Extended Sources Catalog (FHES) by Ackermann et al. [1], the integrated 1 GeV–1 TeV fluxes of resolved high confidence sources in the LAT data extend down to a few/several $\times 10^{-10}$ photons cm^{-2} s^{-1}, while of those which appear point-like and about one magnitude lower, with a median of 2.5×10^{-10} photons cm^{-2} s^{-1}. An estimate for the flux expected from DC 314.8–5.1 due to the interactions with high-energy CRs (assuming no CR overdensity with respect to the CR background), is

$$\begin{aligned} F(>E_\gamma) &\simeq 2\times10^{-13}\,\frac{M/10^5\,M_\odot}{(D/\mathrm{kpc})^2}\left(\frac{E_\gamma}{1\,\mathrm{TeV}}\right)^{-1.7} \\ &\sim 2\times10^{-10}\,\mathrm{photons\,cm^{-2}\,s^{-1}} \end{aligned} \quad (1)$$

[see 8]. In the above, we use $M = 160\,M_\odot$ corresponding to the *total* mass of the cloud, the updated distance $D = 432$ pc, and $E_\gamma = 1$ GeV. This level of emission may be detected in dedicated *Fermi*-LAT studies, leading to a robust estimate of the mass in this pre-stellar, dense dark cloud.

4. Conclusions

The performed pypahdb fitting, originally presented in Kosmaczewski et al. [15], confirms a high ionized fraction within the cloud, ranging from $\simeq 0.5$ within the regions in the closest vicinity

to the ionizing star, down to $\sim 0.3 - 0.4$ at larger distances. Moreover, the PAH emission of the highly ionized regions at the cloud's boundaries, appears to be dominated by large molecules, which become less prevalent for the regions closer to the center of the cloud.

We have supported that DC 314.8–5.1 is a pre-stellar core, with no Class I-III YSO candidates present within the extent of the system down to luminosities as low as $\sim 10^{-4} L_{\odot}$, translating to a stellar core mass down to $0.01 M_{\odot}$ [see 16]. The lack of any YSO detections further supports the claim that cosmic-ray ionization may be playing a part in the processing of the dust of DC 314.8–5.1, as discussed in Kosmaczewski et al. [15]. We also note in this context, that the cloud should be detectable in high-energy γ-rays with *Fermi*-LAT, given the estimate for the total mass of the globule $\sim 160\, M_{\odot}$. Hence, DC 314.8–5.1 remains a pre-stellar cloud core. This makes it an ideal candidate for deeper observations, particularly in high-energy X-ray and γ-ray to study the effects of cosmic-rays on such systems.

Research at the Naval Research Laboratory was supported by NASA DPR S-15633-Y.

References

[1] Ackermann, M., Ajello, M., Baldini, L., et al. 2018, ApJS, 237, 32, doi: 10.3847/1538-4365/aacdf7

[2] Bailer-Jones, C. A. L., Rybizki, J., Fouesneau, M., Demleitner, M., & Andrae, R. 2021, AJ, 161, 147, doi: 10.3847/1538-3881/abd806

[3] Bauschlicher C. W., Ricca A., Boersma C., Allamandola L. J., 2018, ApJS, 234, 32. doi:10.3847/1538-4365/aaa019

[4] Bourke, T. L., Hyland, A. R., Robinson, G., et al. 1995b, MNRAS, 276, 1067, doi: 10.1093/mnras/276.4.1067

[5] Burrows, D. N., Hill, J. E., Nousek, J. A., et al. 2000, in Society of Photo-Optical Instrumentation Engineers (SPIE) Conference Series, Vol. 4140, X-Ray and Gamma-Ray Instrumentation for Astronomy XI, ed. K. A. Flanagan & O. H. Siegmund, 64–75, doi: 10.1117/12.409158

[6] Dunham, M. M. & Vorobyov, E. I. 2012, ApJ, 747, 52. doi: 10.1088/0004-637X/747/1/52

[7] Fazio, G. G., Hora, J. L., Allen, L. E., et al. 2004, ApJs, 154, 10, doi: 10.1086/422843

[8] Gabici, S. 2013, in Astrophysics and Space Science Proceedings, Vol. 34, Cosmic Rays in Star-Forming Environments, ed. D. F. Torres & O. Reimer, 221, doi: 10.1007/978-3-642-35410-6_16

[9] Gaia Collaboration, Brown, A. G. A., Vallenari, A., et al. 2021, A&A, 649, A1, doi: 10.1051/0004-6361/202039657

[10] Gutermuth, R. A., Megeath, S. T., Myers, P. C., et al. 2009, ApJs, 184, 18, doi: 10.1088/0067-0049/184/1/18

[11] Heyer M., Dame T. M., 2015, ARA&A, 53, 583. doi:10.1146/annurev-astro-082214-122324

[12] Houck, J. R., Roellig, T. L., Van Cleve, J., et al. 2004, in Society of Photo-Optical Instrumentation Engineers (SPIE) Conference Series, Vol. 5487, Optical, Infrared, and Millimeter Space Telescopes, ed. J. C. Mather, 62–76, doi: 10.1117/12.550517

[13] Jørgensen J. K., Belloche A., Garrod R. T., 2020, ARA&A, 58, 727. doi:10.1146/annurev-astro-032620-021927

[14] Kang, S.-J., Kerton, C. R., Choi, M., & Kang, M. 2017, ApJ, 845, 21, doi: 10.3847/1538-4357/aa7da3

[15] Kosmaczewski, E., Stawarz, Ł., Rocha, W. R. M., Shenoy, S. S., & Karska, A. 2022, ApJ, 934, 94, doi: 10.3847/1538-4357/ac7a42

[16] Kosmaczewski E., Stawarz L., Cheung C. C., Bamba A., Karska A., Rocha W. R. M., 2023, arXiv, arXiv:2209.02372. doi:10.48550/arXiv.2209.02372

[17] Lada, C. J. 1987, in Star Forming Regions, ed. M. Peimbert & J. Jugaku, Vol. 115, 1

[18] Makovoz, D., Khan, I., & Moshir, M. 2005, PASP, 117, 274, doi: 10.1086/428409

[19] Mizuno, T., Hayashi, K., Metzger, J., et al. 2022, ApJ, 935, 97, doi: 10.3847/1538-4357/ac7de0

[20] Reid I. N., Brewer C., Brucato R. J., McKinley W. R., Maury A., Mendenhall D., Mould J. R., et al., 1991, PASP, 103, 661. doi:10.1086/132866

[21] Rieke, G. H., Young, E. T., Engelbracht, C. W., et al. 2004, ApJs, 154, 25, doi: 10.1086/422717

[22] Robitaille, T. 2019, APLpy v2.0: The Astronomical Plotting Library in Python, doi: 10.5281/zenodo.2567476

[23] Robitaille, T., & Bressert, E. 2012, APLpy: Astronomical Plotting Library in Python, Astrophysics Source Code Library. http://ascl.net/1208.017

[24] Shannon, M. J & Boersma 2018, Proceedings of the 17th Python in Science Conference, 99–105, doi: 10.25080/Majora-4af1f417-00f

[25] Skrutskie M. F., Cutri R. M., Stiening R., Weinberg M. D., Schneider S., Carpenter J. M., Beichman C., et al., 2006, AJ, 131, 1163. doi:10.1086/498708

[26] Smith, J. D. T., Armus, L., Dale, D. A., et al. 2007, PASP, 119, 1133, doi: 10.1086/522634

[27] van den Bergh, S., & Herbst, W. 1975, AJ, 80, 208, doi: 10.1086/111733

[28] Whittet, D. C. B. 2007, AJ, 133, 622, doi: 10.1086/510355

[29] Winston, E., Hora, J., Gutermuth, R., & Tolls, V. 2019, ApJ, 880, 9, doi: 10.3847/1538-4357/ab27c8

[30] Wright, E. L., Eisenhardt, P. R. M., Mainzer, A. K., et al. 2010, AJ, 140, 1868, doi: 10.1088/0004-6256/140/6/1868